Stages of Structural Ordering Leading to Stress Induced Crystallization of PEEK Films: A Mechano-Optical Study on Deformation, Relaxation and Retraction

F. Daver,† A. Blake, and M. Cakmak*

Polymer Engineering Department, University of Akron, Akron, Ohio 44325-0301

Received September 8, 2008; Revised Manuscript Received February 5, 2009

ABSTRACT: Influence of rubbery state large uniaxial deformation followed by relaxation and retraction stages on the mechano-optical behavior of cast amorphous poly(ether ether ketone) films was investigated. At early stage of stretching the birefringence remains linearly proportional to stress. In this linear optical regime, the material remains amorphous. Beyond a critical stress level, a deviation from linearity is observed where a small fraction of the material exhibit extreme preferred orientation with substantial translational disorder resembling nematic-like order. The onset of this deviation also coincides with the onset of strain hardening. Stretching beyond this transition leads to stress induced crystallization. Films stretched to deformation levels well below the onset of strain hardening, remain amorphous before and after the relaxation stages. The entropy reduction gained through deformation of the polymer chains is not sufficient to form crystalline order at short time scales. Once the initial deformation increased beyond the onset of strain hardening, a long-range network of connected crystallites establishes itself.

1. Introduction

Understanding the interactions between processing parameters and the development of structural characteristics is required to control the properties of polymeric materials. Traditional, off-line experimental studies fail to deliver a complete understanding of transitional structural changes during the rapid deformation that takes place in most polymer processing operations involving a high speed stretching of the material. Birefringence as an overall measure of optical anisotropy of materials provides insight into the structural organizations. With the highly instrumented stretching system developed in our group, we have the ability to capture true strain, true stress, and birefringence simultaneously while the samples undergo rapid deformation real time[1−5] This technique has been quite useful in mapping the coupled mechano-optical relationships to large deformations and quantitatively capturing the transitions between amorphous, stress induced crystallization and nematic like order.[5] The formation of intermediate mesophase order in PET, PP, and poly(diethylsiloxane) under flow has been extensively reviewed by Li and Jeu[6] recently. We refer the reader to this excellent review for all pertinent literature in the subject. They anticipated the formation of such intermediate structures in semirigid polymers like PEEK particularly as a result of flow under conditions where the relaxations are highly restricted.

This paper represents our continuing efforts to understand the mechano optical behavior of different classes of polymers including semirigid polymers with slow crystallization character such as PET,[1] PEN,[2] PEN/PEI blends[3] PEN−nanocomposites,[7] PMMA/PB-Cl blends,[8] and flexible fast crystallization polypropylene.[9]

PEEK with its excellent mechanical properties, good solvent resistance, and very high temperature resistance is of significant scientific and industrial importance.[10] It belongs to group polymers that exhibit slow thermal crystallization character due to its high chain rigidity leading to T_g well above the room temperature. The polymers that belong to this group can easily be quenched into glassy state with normal melt casting technique and they remain stable at room temperature.

This material is useful for high temperature applications for magnetic disks[11] capacitors, electric insulators.[12] Various processing effects have been studied. These include deformation below glass transition temperature[13] and uni- and biaxial stretching effects on surface roughness and thickness uniformity.[14] The influence of deformation on the structure of PEEK has been studied by several authors using stretch-stop-measure techniques in rubbery or cold stretching temperatures. These studies concentrated on IR Raman spectroscopy, X-ray diffraction, and thermal analysis for evolution of phase behavior, chain conformation as influenced by deformation conditions.[15−18]

The birefringence technique has been successfully applied to study the development of structural characteristic for both homopolymers and blends of PEEK[19−21] during annealing from preoriented state. However, the real-time mechano-optical behavior of PEEK films during deformation in the rubbery state from amorphous precursors has not been investigated. This is the focal point of interest in this paper. The real time studies are also augmented with off-line structural measurement techniques to elucidate the molecular mechanisms associated with the transitions observed in mechano-optical behavior during deformation, relaxation and retraction stages in an effort to shed light into stages leading to stress induced crystallization.

2. Experimental Procedures

2.1. Material. Commercial grade (381G) PEEK cast film of 100 μm thickness was kindly provided by Victrex. As-received melt cast samples were essentially amorphous (∼12% crystallinity) as measured by DSC. Upon heating at 20 °C/min heating rate they exhibit glass transition temperature (T_g) at 144 °C; a cold crystallization (T_{cc}) peak was observed at 172 °C and melt temperature (T_m) at 342 °C. The rubbery state is situated between 144 and 172 °C. In these studies, we concentrate all of our studies roughly equidistant between these two temperatures at 155 °C to avoid complications that occur either of the above transitions (thermal crystallization at higher temperature and glassy behavior at lower temperatures).

* Corresponding author. E-mail: cakmak@uakron.edu.
† Present address: RMIT University, School of Aerospace, Mechanical and Manufacturing Engineering, Bundoora, Victoria 3083, Australia.

10.1021/ma802041n CCC: $40.75
Published on Web 03/19/2009

2.2. Online Birefringence and True Mechanical Behavior Measurements. A uniaxial stretching machine developed in our group was used to simultaneously determine the mechano-optical properties of the PEEK films during deformation and relaxation processes. The machine composed of three parts: (1) the uniaxial stretching machine and environmental chamber, (2) the spectral birefringence systems, and (3) a laser-based width-measurement system. The uniaxial stretching machine is designed to allow the two cross-heads to move in opposite directions, so that the measurements are always made in the stationary midsection of the dumbbell shaped samples. Time variation of the local thickness in the stationary midsection is calculated assuming simple uniaxial symmetry,

$$\frac{W_t}{W_0} = \frac{D_t}{D_0} \tag{1}$$

where W is the width measured by real time precision laser micrometer and D is the thickness. Subscript 0 refers to the initial conditions. The validity of uniaxial symmetry assumption in these samples was checked by comparing predicted thickness from the online data and experimentally determined off-line data. They follow the expected linear correlation with each other following uniaxial assumption (data are not shown).

The local true strain in the midpoint is calculated as

$$\text{true strain (Hencky)} = \ln\left(\frac{L_t}{L_0}\right) = \ln\left(\frac{W_0}{W_t}\right)^2 \tag{2}$$

Similarly, the true stress at the midpoint is

$$\text{true stress} = \sigma_T = \frac{F_t}{(W_t \times D_t)} = \frac{F_t}{\left(\frac{W_t^2 \times D_0}{W_0}\right)} \tag{3}$$

where F_t is the force at the clamps at time t. Using the above methodology, birefringence and true mechanical response of the films can be determined in real-time.

The birefringence measurements were taken at 546 nm wavelength. Further details of the online birefringence system can be found elsewhere.[22−24]

2.3. Sample Preparation. Dumbbell-shaped samples were cut from the sheets of "as-cast" amorphous film. The samples were 70 mm long × 40 mm wide, and 30 mm wide in the narrowest region. The samples were clamped and mounted on the uniaxial stretching system inside an environmental chamber. The distance between the clamps was 30 mm.

2.4. Experimental Conditions. After clamping, the samples were equilibrated at 155 °C for 10 min before commencing the deformation. Initially, a series of strain rates 2, 20, 100, 200, and 300 mm/min and stretching ratios up to 3× were employed. All other experimental studies were conducted at 20 mm/min strain rate and up to a stretch ratio of 3×.

In order to investigate the effect of prestretching prior to relaxation and retraction three sets of tests were conducted:

1. Stretching to 1.25×, 1.5×, 1.8×, 2.2×, 2.5× and 3× engineering stretch ratios followed by rapid cooling without relaxation period. In the following Results and Discussion section, we will only report the true strains obtained using these engineering stretch ratios.

2. Stretching followed by a relaxation period at the stretching temperature of 155 °C. A fixed 15 min relaxation was employed. For the stretch ratio of 1.5× an additional relaxation period of 1 h was employed.

3. Stretching was followed by retraction, and then 15 min relaxation at 155 °C. The retraction was 5% for stretch ratios of 2.2× and 2.5× and 8% for 3×.

All these experiments were carried out with 20 mm/min initial strain rate.

Thermal Characterization. The thermal properties of the PEEK films were measured using differential scanning calorimetry (DSC); the instrument was 2920 MDSC V2.2A TA. Samples of approximately 3−4 mg were crimped in aluminum pans and were scanned at a heating rate of 10 °C/min in a dry nitrogen atmosphere. The thermal properties referred to the maximum peak positions. The degree of crystallinity was determined using eq (4) considering the heat of fusion of 100% crystalline (ΔH_f^o) to be 130 J/g.[10,25]

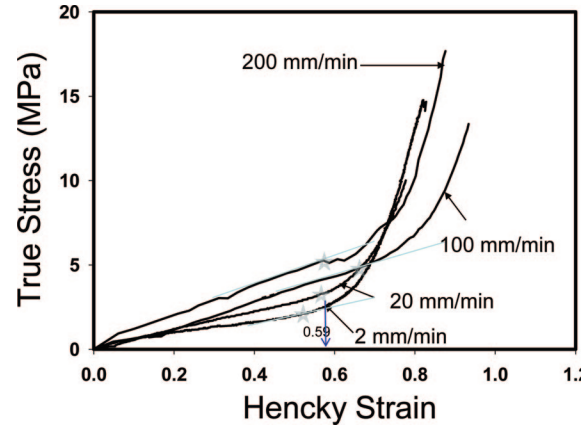

Figure 1. True stress versus Hencky strain curves at different stretch rates at 155 °C (indicates the onset of strain hardening).

$$\chi\,(\%) = \frac{(\Delta H_m - \Delta H_c)}{\Delta H_f^o} \tag{4}$$

ΔH_m and ΔH_c are the enthalpy of melting and the enthalpy of crystallization respectively.

Wide-Angle X-ray Diffraction (WAXS) Measurements. A Bruker AXS generator equipped with a copper target tube and two-dimensional detector was used to obtain one-quadrant WAXS patterns of the samples. The generator was operated at 40 kV and 40 mA with a beam monochromatized to Cu Kα radiation. For all experiments the sample-to-detector distance was kept at 11.5 cm, and the exposure time was set at 10 min.

3. Results and Discussion

3.1. True Mechanical Behavior in Rubbery State. In order to investigate the influence of stretching rate on the structural evolution mechanism during uniaxial stretching of PEEK, samples were stretched at 2, 20, 100, 200 mm/min as shown in Figure 1. All samples show strain hardening: a steep increase in stress is observed once the strain reaches a critical value. The increase of strain rate first delays the onset of strain hardening to larger strain levels and beyond 100 mm/min the strain at the onset of strain hardening decreases. With the help of a pyrometer, potential adiabatic temperature rise in the samples were monitored during stretching. This rise was found to be no more than about 0.5 °C above the set 155 °C temperature at high stretching rates. This indicates that the stretching is essentially isothermal in the stretching rate range investigated.

The strain optical behavior of these samples depends on the deformation rate and the large deformation behavior is certainly nonlinear particularly at lower strain rates as illustrated in Figure 2. However, we observe that at higher rates the initial slope of these curves tends to approach one asymptote value and become linear (note the data for 200 mm/min). This suggests that significant reduction in chain relaxation during deformation with the increase of strain rate leads to gradual approach to linear correlation between macroscopic strain as measured by true strain and molecular level strains as measured by birefringence. The level of birefringence obtained at lower strain rates are always lower as the orientation

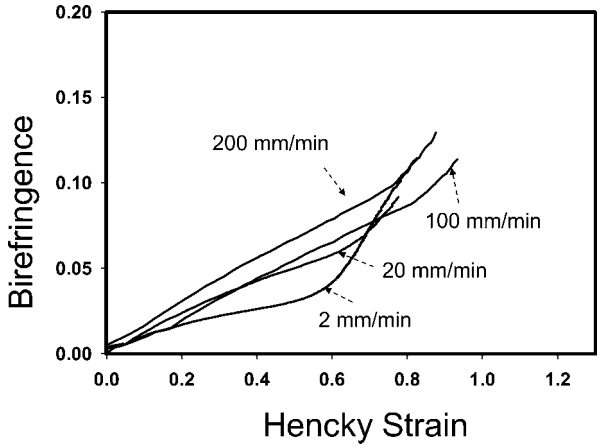

Figure 2. Birefringence vs Hencky strain as influenced by strain rate at 155 °C processing temperature.

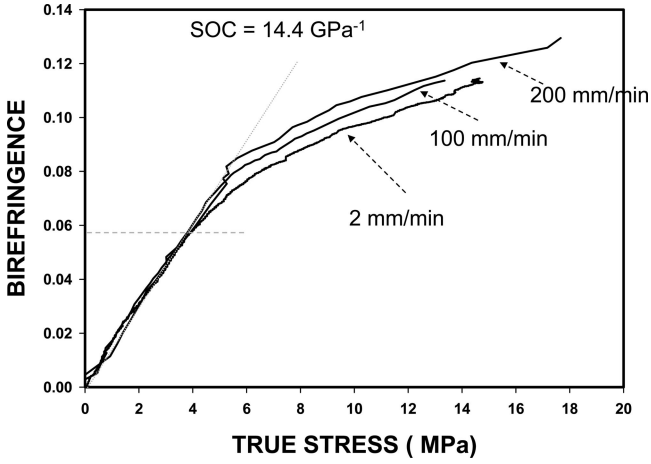

Figure 3. Birefringence vs true stress as influenced by strain rate at 155 °C processing temperature.

relaxation becomes pronounced as compared to the orientation behavior during deformation. Another interesting point on strain optical behavior is the observation of crossover points in these curves. This is as a result of increase of slope of final stages of these curves with decreasing strain rate. We suspect this is related to the differences in the formation of structural hierarchy in the materials. Lower stretching rate could lead to the formation of orientation induced nuclei as the accompanying relaxation becomes prominent and this leads to the formation of crystalline nuclei junctions that—in turn—establish a long-range physical network that rapidly tighten up and leading to rapid increase in orientation and thus rapid birefringence rise. It appears that the key in this process is the time given for orientation relaxation during deformation. If amply provided, this leads to acceleration of the formation of stress induced nuclei. To validate these propositions, structural studies are needed, and they are presented in following sections.

Large deformation stress optical behavior shown in (Figure 3) indicates a rate independent initial linear stress optical behavior with a slope defining the stress optical constant $C = 14.4\ \mathrm{GPa}^{-1}$. Beyond about 5 MPa deviations from the initial linear behavior is observed. The use of higher stretching rates leads to higher birefringences. However, they all eventually tend to plateau at higher stresses. To assess the structural mechanisms responsible for each regime observed in the stress and strain optical curves, we elected to investigate the behavior of the samples at 20 mm/min strain rate and prepared a series of samples with varying deformation levels and rapidly cooled them under constraint to room temperature to lock-in the structure. These samples were then analyzed off line by WAXS and differential scanning calorimetry. The integrated data are shown in Figure 4 together with WAXS patterns as well as crystallinity as extracted from DSC curves. Horizontal dash lines were drawn to aid the eye the corresponding locations of each region of interest for both stress optical and strain optical behaviors plotted in these graphs. The wide-angle X-ray diffraction (WAXS) patterns of the stretched samples are given in Figure 4. At true strain of $\varepsilon_H = 0.33$ they indicate the existence of an amorphous halo. An initial linear increase in birefringence is observed until a true strain of $\varepsilon_H = 0.58$, beyond which the slope negatively deviates from this linearity. This is the point where we also observe the onset of strain hardening at true stress−strain curves shown in Figure 1. In the WAXS pattern at this location we observe a very sharp equatorial spot (whose location is indicated by an arrow) superimposed on top of an amorphous halo. This is a clear indication of sudden appearance of highly oriented population of polymer chains exhibiting significant translational disorder along their axes. The regions where such order is present exhibit near perfect chain orientation. Additionally the amorphous halo exhibit very low anisotropy so these very highly oriented regions are highly localized and are suspected to form a long-range connected internal networks. Otherwise they may not achieve such super high orientation levels. Obviously, at this point in the deformation, the three-dimensional crystalline order is not formed as evidenced by the absence of off-equatorial crystalline diffraction peaks. With continuing increase in deformation up to $\varepsilon_H = 0.81$ a long-range three-dimensional order is established as demonstrated by the clear appearance of equatorial (200) and the off-equatorial (111) crystalline peak. Further increase in deformation sharpens the crystalline peaks without significantly altering the crystalline orientation behavior.

The crystallinity values of the samples as a function of true strain are also shown in Figure 4. Following a steep increase at the true strain of $\varepsilon_H = 0.71$, crystallinity levels off at 23%. Figure 5 shows the differential scanning calorimetry (DSC) scans of these samples stretched at 20 mm/min at 155 °C. The cold crystallization peak (T_{cc}) shifts to lower temperatures until about the true strain of $\varepsilon_H = 0.75$ and then it levels off. The decrease in T_{cc} can be explained by a decrease in the conformational entropy of the polymer chains as a result of preferential orientation under deformation and an increase in the driving force for crystallization. Crystallization therefore takes place at lower temperatures as evidenced by DSC thermograms.

3.2. Influence of Relaxation on the Strain Induced Structural Ordering Process. In a previous study on polylactic acid,[5] we have shown that the increase of strain rate leads to prevention of oriented crystallization in that high molecular weight polymer due to substantial decrease of chain relaxation with the increase of strain rate or decrease of stretching temperature. In this study, the material of interest is a condensation polymer with much lower molecular weight, and we wanted to explore the influence of relaxation and forced retraction immediately following deformation on the phase formation in the materials.

Figure 6 shows the true stress−true strain and birefringence true strain behavior of samples that were stretched to a series of deformation levels below the onset of strain hardening. As illustrated in Figure 6 a, the sample stretched to the lowest deformation level (the true strain of $\varepsilon_H = 0.18$) show rapid relaxation of both stress and birefringence in 15 min constrained holding period. Toward the end of relaxation there is slight appearance on increase of strain. At the true strain of about $\varepsilon_H = 0.37$, the same initial behavior is observed at the start of the relaxation however, beyond a critical point the strain begins to increase even though the sample clamp separation is maintained

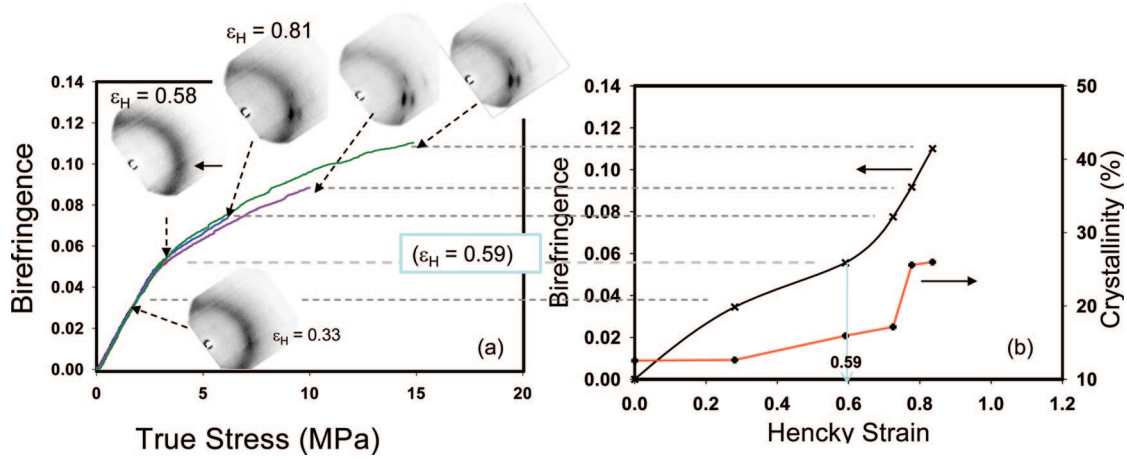

Figure 4. For samples drawn at 20 mm/min and 155 °C (a) Birefringence versus true stress. (b) Birefringence and crystallinity versus Hencky strain (ε_H) (0.59 = strain at onset of strain hardening from Figure 1 exactly coinciding with that observed here).

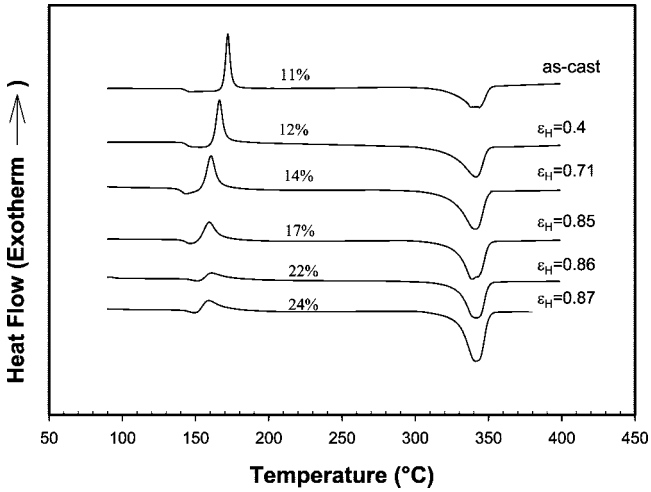

Figure 5. DSC thermographs of samples drawn at 20 mm/min and 155 °C. Hencky strains and % crystallinities are shown.

constant (meaning that under the action of the stresses built up during deformation, the middle of the sample begins to deform (graphically shown in this figure as the symmetry center of the sample)). As the strain increases. so does the birefringence. This behavior becomes even more pronounced at the true strain of $\varepsilon_H = 0.53$. This is the "spontaneous deformation" phenomenon captured by our real time measurement system. In order to explore what happens during the relaxation processes, we have subjected the samples strained to the true strain of $\varepsilon_H = 0.4$ to a series of relaxation times at the stretching temperature and subsequently rapidly cooled to room temperature to assess their birefringence and molecular order developed up to that condition. Figure 7 shows the temporal development of birefringence for each sample tested together with the WAXS pattern at the end of each experiment. Although the samples are rapidly cooled to room temperature, there may have been slightly further increase in relaxation in cooling stage. This is not expected to cause significant changes in the structure of the samples between the end of relaxation and end of cooling as temperature differential between the processing temperature 155 °C and room temperature 22 °C is quite large and our processing temperature is only 10 °C above the glass transition temperature.

At the end of deformation, the sample exhibits an amorphous halo with slight evidence of equatorial sharp peak superposed on the primary amorphous halo. As the relaxation progresses, birefringence decrease accompanies the definition of the equatorial sharp peak. This equatorial sharp peak becomes more prominent particularly beyond the birefringence minimum (7 and 15 min). In the absence of any other peaks, this peak indicates the development of a chain population of extremely high orientation and with significant translational disorder along the chain axis. The stress optical behavior of the same set of data is shown in Figure 8. As noted in this figure, the stretching stage is essentially linear following the stress optical behavior and follows the stipulation that the crystallization does not develop during stretching (note the 0 min WAXS data). During the relaxation, birefringence-stress data doubles back along the same curve until about 5 min where the equatorial sharp peak (denoted by the arrow) begins to be dominant and beyond this point the deviation from linear stress optical rule is noted. At this stage, the final sample also show an increase in crystallinity though still remaining at fairly low 16−19% levels (indicated with each WAXS pattern Figure 8).

If sufficiently long time is given during relaxation we do observe the formation of crystalline phase even at $\varepsilon_H = 0.18$ deformation level (see Figure 9 $\varepsilon_H = 0.18$ 1 h relaxation WAXS pattern). This is partly due to the proximity of the processing temperature to thermal crystallization (cold crystallization) temperature (Figure 5) when given sufficiently long time become effective in converting oriented chains to crystalline state. Note the absence of completely disoriented crystalline phase at the latter pattern indicating that only those that have retained some orientation levels become crystalline. If we had waited much longer at this temperature, we would have satisfied the conditions for the unoriented polymer chains to thermally crystallize and we would have seen the complete circles on the crystalline peak locations in WAXS patterns. Increase of initial deformation to $\varepsilon_H = 0.53$, certainly amplifies the above observed behavior and following the stretching and relaxation we observe a complete three-dimensional crystalline order in the sample with $\varepsilon_H = 0.53$ shown in Figure 9).

3.3. Relaxation Studies (at High Strain Levels, near and above the Onset of Strain Hardening). Following the relaxation studies conducted in the initial linear region of the stress−strain deformation curves, the samples were stretched up to $\varepsilon_H = 0.66$ and $\varepsilon_H = 0.87$. One set of samples was held constrained after stretching 15 min immediately after stretching; another set underwent a small retraction, and then 15 min of constrained holding followed.

The true stress strain data and birefringence true strain data are shown in Figure 10 for sample stretched to $\varepsilon_H = 0.66$. As indicated in the graph, the relaxation stage still accompanies small additional deformation under the action of built up stresses

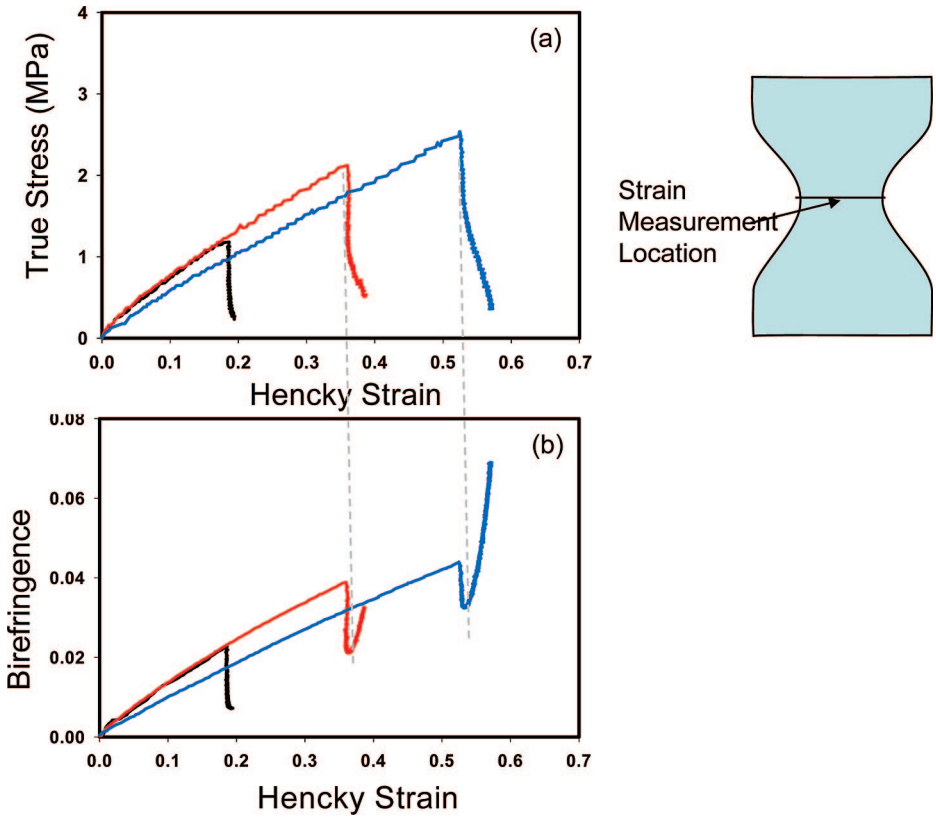

Figure 6. (a) True stress−strain. (b) Birefringence versus true strain for samples drawn below the onset of strain hardening followed by 15 min of constrained relaxation.

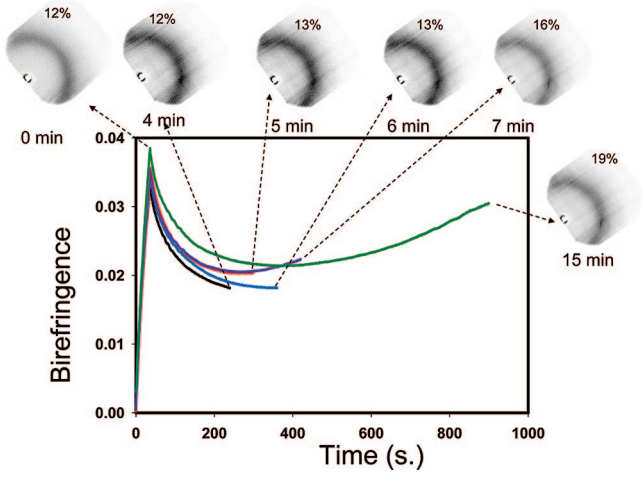

Figure 7. Effect of holding time on birefringence of samples drawn to $\varepsilon_H = 0.4$ at 20 mm/min (% crystallinities are indicated on each WAXS pattern).

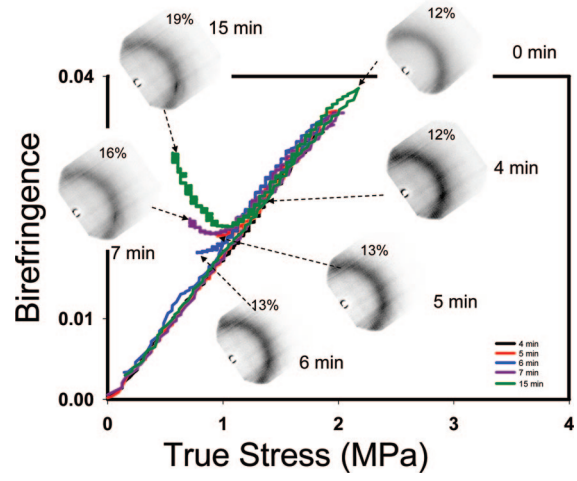

Figure 8. Stress optical behavior of films stretched to $\varepsilon_t = 0.5$ at 20 mm/min and 155 of constrained relaxation times.

during deformation even though the crosshead movement ceases at the start of the constrained relaxation phase. At the latter stage, a short relaxation is followed by a rise in birefringence as indicated in Figure 10b. If we apply a rapid 8% strain retraction, the true stress, true strain as well as birefringence decreases temporarily. In the ensuing constrained relaxation stage, the strains at the midpoint of the sample where all measurements are made, recover and birefringence rapidly rises though it does not reach the levels exhibited by sample that went through relaxation only. The stress optical behavior of the latter set is shown in Figure 11 together with WAXS data taken at the end of stretching, at the end of retraction and at the end of relaxation. As compared to stretching and retraction phases, there are no discernible differences in structure between the stretching and retraction stages. They both exhibit a phase with sharp chain orientation possessing low translational order along the chain axes. In both cases, the long-term relaxation converts these structures to an oriented crystalline domains exhibiting good three-dimensional order as the off-equatorial peaks appear. In the retraction stage, some recovery of the oriented amorphous chains occurs as evidenced by a decline in birefringence (Figure 11b) but without significant influence on the orientation of the crystallized regions. At the end of both processes, we see almost no difference in final crystallinities as shown in Figure 12.

Figures 13 and 14 show the true stress-strain and birefringence-strain data on sample stretched to true strain of about 0.85. Since this condition is well beyond the onset of strain hardening, there is very little increase in strain during relaxa-

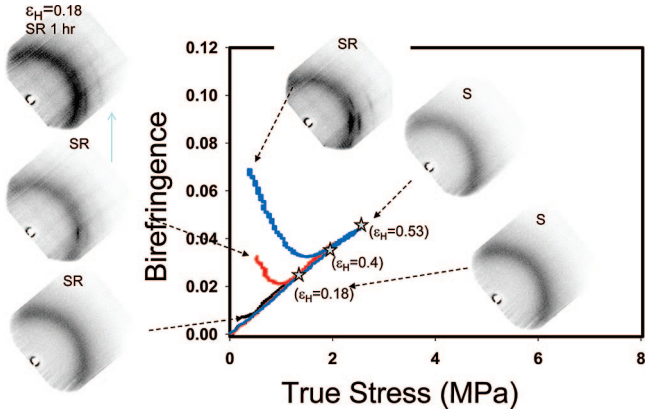

Figure 9. True stress versus birefringence for samples drawn below the onset of strain hardening followed by 15min of constrained relaxation. ($\varepsilon_H = 0.18$) has an extra WAXS pattern at 1 h constrained holding showing start of oriented crystallization) (S = stretched; SR+ stretched and relaxed).

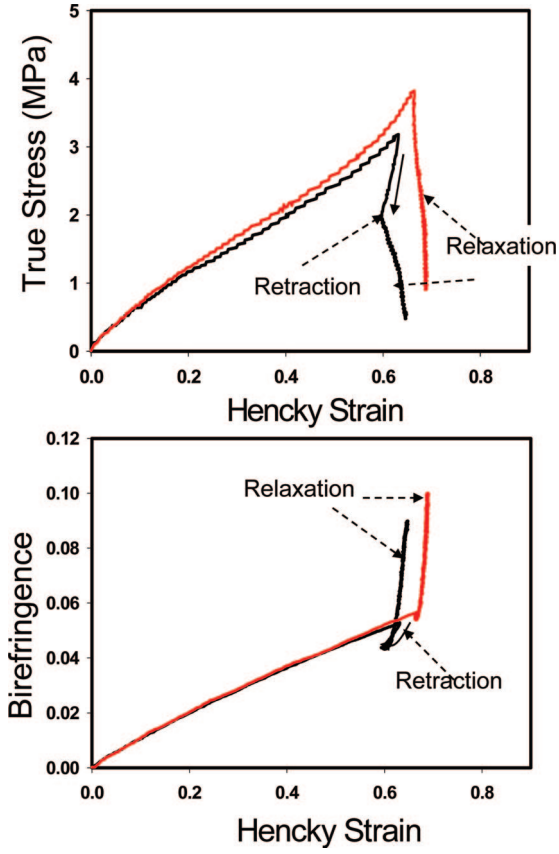

Figure 10. (a) True stress−strain. (b) Birefringence versus Hencky strain for samples drawn above the onset of strain hardening at $\varepsilon_H = 0.66$ followed by relaxation and 8% strain retraction followed by 15 min of constrained relaxation.

tion, and following 5% retraction as birefringence continues to increase. Stress optical behavior (Figure 15 and 16) and accompanying WAXS patterns indicate that the retraction causes the decrease of birefringence and stress. The ensuing relaxation stage rapidly develops the oriented crystallization process. Remarkably, there is almost no difference between the WAXS patterns of samples, only relaxed and retracted and relaxed. This could only mean that the most of the retraction is absorbed primarily by the amorphous regions presumably elastically stored strains are recovered while the long-range connected crystalline regions remained intact and little to no changes has taken place in it. We suspect that the relaxation simply helped

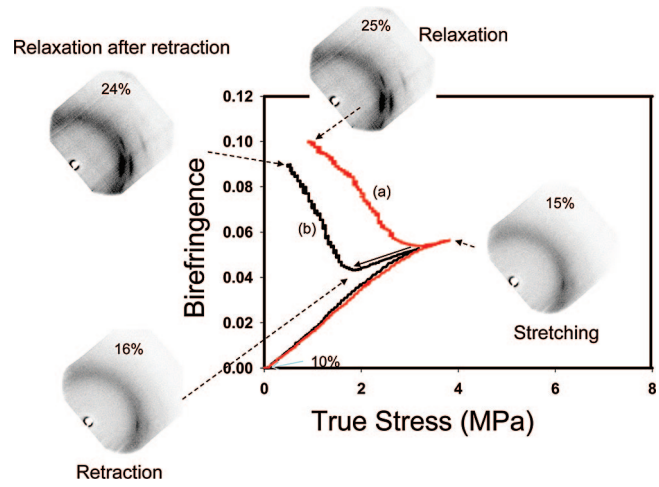

Figure 11. WAXD patterns and true stress versus birefringence curves of samples stretched to (a) $\varepsilon_H = 0.66$ followed by relaxation; (b) followed by retraction and relaxation.

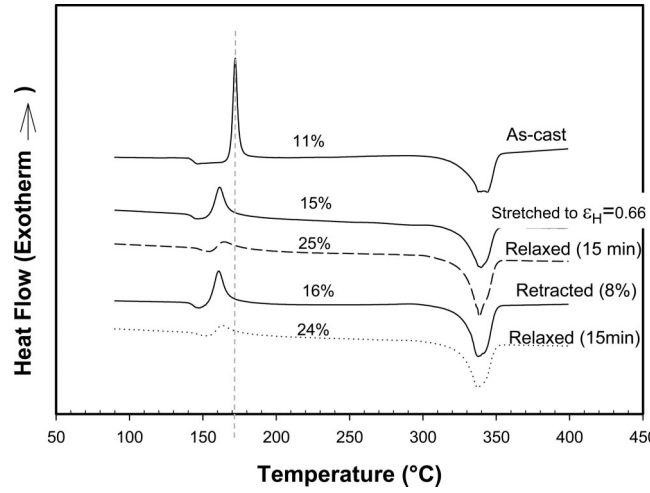

Figure 12. DSC thermogram of PEEK samples drawn at 20 mm/min at 155 °C: as-cast; stretched to $\varepsilon_H = 0.66$; constrained relaxed for 15 min after stretching; retracted 8% after stretching; constrained relaxed after retraction.

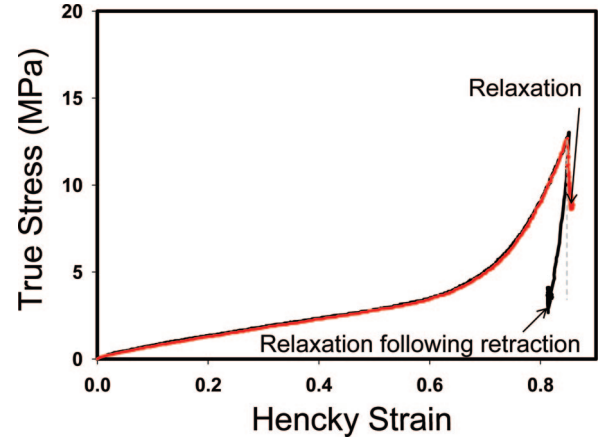

Figure 13. (a)True stress−strain behavior in PEEK film stretched to $\varepsilon_H = 0.87$ engineering stretch ratio at 20 mm/min stretching rate at 150 °C followed by 15 min of constrained relaxation.

in the additional growth of the already existing crystalline regions instead of causing nucleation and unoriented crystal growth. An important point to note that the retraction stage did not lead to formation of highly disoriented crystalline regions

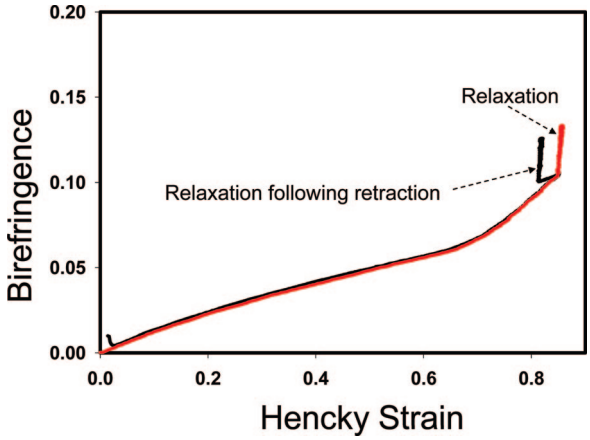

Figure 14. Birefringence−Hencky strain, behavior in PEEK film stretched to $\varepsilon_H = 0.85$ at 20 mm/min stretching rate at 150 °C followed by 15 min relaxation only and 5% strain retraction followed by 15 min of constrained relaxation.

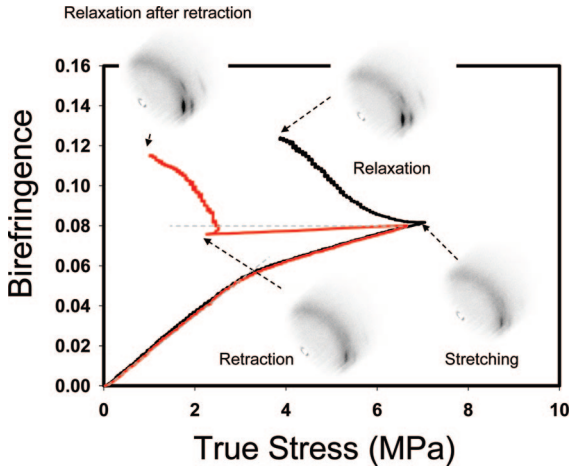

Figure 15. Stress optical behavior of in PEEK film stretched to $\varepsilon_H = 0.85$ at 20 mm/min stretching rate at 150 °C followed by 15 min relaxation only and 8% strain retraction followed by 15 min of constrained relaxation.

as this is absent in Figure 15 and in the data presented earlier. If the samples are stretched to very large deformation levels ($\varepsilon_H = 0.85$), the crystalline order develops during this stretching phase. Relaxation increases the crystallinity from 18 to 27%. Birefringence decrease accompanies the retraction phase, and following this the stress increases for a brief time without accompanying birefringence increase. Subsequently, the birefringence rapidly develops, but it does not reach the same level as the stretching and relaxation step.

4. Conclusions

Coupled mechano optical behavior of cast amorphous PEEK films in their rubbery state allowed us to identify structural ordering sequence that takes place during deformation. In the initial stage of uniaxial deformation, the samples remained amorphous following the linear stress optical behavior. Beyond this linear stage, negative deviation is observed in the stress optical behavior accompanied by the appearance of nematic-like order in which the chains attain near perfect orientation with substantial translational disorder along the chain axis directions. Onset of strain hardening also was found to coincide with the appearance of these nematic-like ordered regions that constitute the nodes of the long-range connected network.

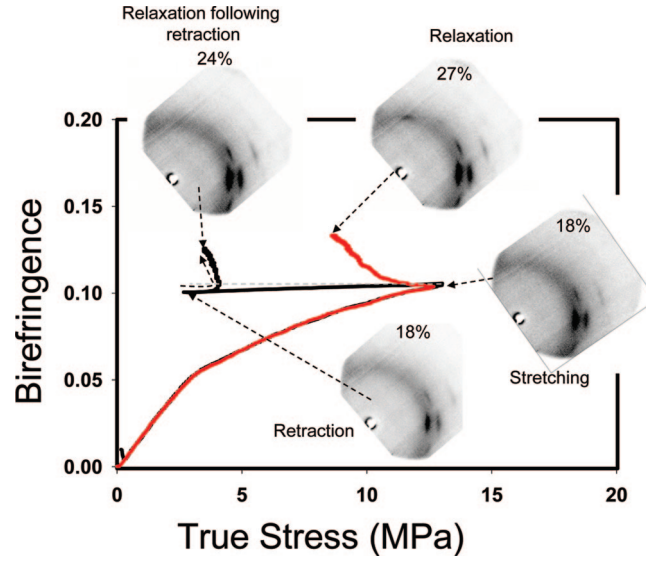

Figure 16. Stress optical behavior of in PEEK film stretched to $\varepsilon_H = 0.87$ at 20 mm/min stretching rate at 150 °C followed by 15 min relaxation only and 8% strain retraction followed by 15 min of constrained relaxation.

Constrained relaxation and deliberate small retraction have pronounced effects on the structural transitions. If the long-range connected network has not formed during deformation, the relaxation stage leads to complete disorientation and no crystallization. Once the initial elements of network formed at higher deformations, the relaxation stage ultimately nucleates the crystalline nodes that completes the connections of this three-dimensional network, and this leads to oriented crystallization.

Acknowledgment. We would like to thank Mr. Mike Percy of Victrex plc. for providing cast PEEK films.

Supporting Information Available: Figures showing Hencky strain vs pyrometer temperature and Hencky strain and strain rate vs time. This material is available free of charge via the Internet at http://pubs.acs.org.

References and Notes

(1) Martins, C. I.; Cakmak, M. *Polymer* **2007**, *48*, 2109–2123.
(2) Martins, C.; Cakmak, M. *Macromolecules* **2006**, *39*, 4824–4833.
(3) Kanuga, K.; Cakmak, M *Macromolecules* **2005**, *38*, 9698–9710.
(4) Martins, C. I.; Cakmak, M. *Macromolecules* **2005**, *38*, 4260–4273.
(5) Mulligan, J.; Cakmak, M. *Macromolecules* **2005**, *38*, 2333–2344.
(6) Li, L.; DeJeu, W. H. *Adv. Polym. Sci.* **2005**, *181*, 75–120.
(7) Kanuga, K.; Cakmak, M. *Polymer* **2007**, *48*, 7176–7192.
(8) Yalcin, B.; Cakmak, M.; Arin, A. H.; Hazer, B.; Erman, B. *Polymer* **2006**, *47*, 8183.
(9) Koike, Y.; Cakmak, M. *J. Polym. Sci., Polym. Phys.* **2006**, *44*, 925–941.
(10) Cakmak, M. Polyaryl ether ketones: properties and structure development. In *Handbook of thermoplastics*; Olabisi, O., Ed.; Marcel Dekker: New York, 1997.
(11) Kato, H; Hamano, H.; Hasegawa, K.; Nomi, N. (Teijin Ltd., Japan). Jpn. Kokai Tokkyo Koho (1990), 9 pp. CODEN: JKXXAF JP 02037519 A 19900207.
(12) Hasegawa, K.; Nomi, Norihiro ; Hamano, Hisashi ; Kato, Hideo. (Teijin Ltd., Japan). Jpn. Kokai Tokkyo Koho (1989), 11 pp JP 01101336 A 19890419 Heisei.
(13) Karbach, A. *Polym. Commun.* **1987**, *28* (1), 24–27.
(14) Cakmak, M.; Simhambhatla, M. *Polym. Eng. Sci.* **1995**, *35*, 1562–1568.
(15) Voice, A. M.; Bower, D. I.; Ward, I. M. *Polymer* **1993**, *34*, 1164–1173.
(16) Everall, N. J.; Chalmers, J. M.; Ferwerda, R.; van der Maas, J. H.; Hendra, P. J. *J. Raman Spectrosc.* **1994**, *25* (1), 43–51.

(17) Blundell, D. J.; Mahendrasingam, A.; McKerron, D.; Turner, A.; Rule, R.; Oldman, R. J.; Fuller, W. *Polymer* **1994**, *35*, 3875–3882 .
(18) Wang, S. G.; Liu, T. X.; Mo, Z. S.; Wang, J. Z.; Xu, F.; Wu, Z. W. *Macromol. Rapid Commun.* **1997**, *18* (2), 83–91.
(19) Bassingy, V.; Séguéla, R.; Rietsch, F.; Jasse, B. *Polymer* **1993**, *34*, 4052.
(20) Bicakci, S.; Cakmak, M. *Polymer* **2001**, *43*, 149.
(21) Zhou, X.; Cakmak, M. *Polymer* **2006**, *47*, 8183.
(22) Serhatkulu, T. F.; Cakmak, M. *SPE Antec Tech. Pap.* **1999**, *1645*.
(23) Korkturk, G.; Serhatkulu, T. F.; Cakmak, M. *SPE Antec Tech. Pap.* **2000**, *1737*.
(24) Toki, S.; Valladares; Sen, T. Z., Cakmak, M. *Antec Tech. Pap.* **2001**, *1830*.
(25) Bicakci, S.; Cakmak, M. *Polymer* **2002**, *43*, 2737.

MA802041N